

Retinexformer: One-stage Retinex-based Transformer for Low-light Image Enhancement

Yuanhao Cai^{1,2}, Hao Bian^{1,2}, Jing Lin^{1,2},
Haoqian Wang^{1,2,✉}, Radu Timofte^{3,4}, Yulun Zhang⁴

¹ Shenzhen International Graduate School, Tsinghua University,

² Shenzhen Institute of Future Media Technology, ³ University of Würzburg, ⁴ ETH Zürich

Abstract

When enhancing low-light images, many deep learning algorithms are based on the Retinex theory. However, the Retinex model does not consider the corruptions hidden in the dark or introduced by the light-up process. Besides, these methods usually require a tedious multi-stage training pipeline and rely on convolutional neural networks, showing limitations in capturing long-range dependencies. In this paper, we formulate a simple yet principled One-stage Retinex-based Framework (ORF). ORF first estimates the illumination information to light up the low-light image and then restores the corruption to produce the enhanced image. We design an Illumination-Guided Transformer (IGT) that utilizes illumination representations to direct the modeling of non-local interactions of regions with different lighting conditions. By plugging IGT into ORF, we obtain our algorithm, Retinexformer. Comprehensive quantitative and qualitative experiments demonstrate that our Retinexformer significantly outperforms state-of-the-art methods on seven benchmarks. The user study and application on low-light object detection also reveal the latent practical values of our method. Codes and pre-trained models will be released.

1. Introduction

Low-light image enhancement is an important yet challenging task in computer vision. It aims to improve the poor visibility and low contrast of low-light images and restore the corruptions (e.g., noise, artifact, color distortion, etc.) hidden in the dark or introduced by the light-up process. These issues challenge not only human visual perception but also other vision tasks like nighttime object detection.

Hence, a large number of algorithms have been proposed for low-light image enhancement. Plain methods like histogram equalization and gamma correction tend to produce undesired artifacts because they barely consider the illumination factors. Traditional cognition methods rely on the Retinex theory [28] that assumes the color image can be decomposed into two components, *i.e.*, reflectance and illu-

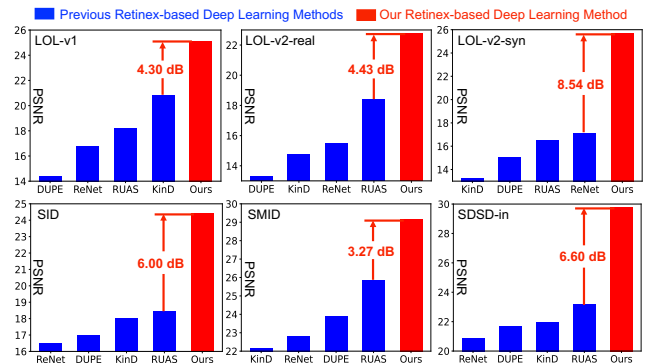


Figure 1. Our Retinexformer significantly advances state-of-the-art Retinex-based deep learning methods including DUPE (Deep-UPPE [48]), ReNet (RetinexNet [53]), KinD [65], and RUAS [31] on six low-light image enhancement benchmarks: LOL-v1 [53], LOL-v2 [58]-real, LOL-v2 [58]-synthetic, SID [8], SMID [9], and SDSD [47]-indoor. Especially on the SDSD-indoor, SID, and LOL-v2-synthetic datasets, the improvements are over **6 dB**.

mination. Different from plain methods, traditional methods focus on illumination estimation but usually introduce severe noise or distort color locally because these methods assume that the images are noise- and color distortion-free. This is inconsistent with real under-exposed scenes.

With the development of deep learning, convolutional neural networks (CNNs) have been applied in low-light image enhancement. These CNN-based methods are mainly divided into two categories. The first category directly employs a CNN to learn a brute-force mapping function from the low-light image to its normal-light counterpart, thereby ignoring human color perception. This kind of methods lack interpretability and theoretically proven properties. The second category is inspired by the Retinex theory. These methods [53, 64, 65] usually suffer from a multi-stage training pipeline. They employ different CNNs to decompose the color image, denoise the reflectance, and adjust the illumination, respectively. These CNNs are first trained independently and then connected together to be finetuned end-to-end. The training process is tedious and time-consuming.

In addition, these CNN-based methods show limitations in capturing long-range dependencies and non-local self-similarity, which are critical for image restoration. The recently rising deep learning model, Transformer, may provide a possibility to address this drawback of CNN-based methods. However, directly applying original vision Transformers for low-light image enhancement may encounter an issue. The computational complexity is quadratic to the input spatial size. This computational cost may be unaffordable. Due to this limitation, some CNN-Transformer hybrid algorithms like SNR-Net [56] only employ a single global Transformer layer at the lowest spatial resolution of a U-shaped CNN. Thus, the potential of Transformer for low-light image enhancement still remains under-explored.

To cope with the above problems, we propose a novel method, Retinexformer, for low-light image enhancement. Firstly, we formulate a simple yet principled One-stage Retinex-based Framework (ORF). We revise the original Retinex model by introducing perturbation terms to the reflectance and illumination for modeling the corruptions. Our ORF estimates the illumination information and uses it to light up the low-light images. Then ORF employs a corruption restorer to suppress noise, artifacts, under-/over-exposure, and color distortion. Different from previous Retinex-based deep learning frameworks that suffer from a tedious multi-stage training pipeline, our ORF is trained end-to-end in a one-stage manner. Secondly, we propose an Illumination-Guided Transformer (IGT) to model the long-range dependencies. The key component of IGT is Illumination-Guided Multi-head Self-Attention (IG-MSA). IG-MSA exploits the illumination representations to direct the computation of self-attention and enhance the interactions between regions of different exposure levels. Finally, we plug IGT into ORF as the corruption restorer to derive our method, Retinexformer. As shown in Fig. 1, our Retinexformer surpasses state-of-the-art (SOTA) Retinex-based deep learning methods by large margins on various datasets. Especially on SID [8], SDS [47]-indoor, and LOL-v2 [58]-synthetic, the improvements are over **6 dB**.

Our contributions can be summarized as follows:

- We propose a novel Transformer-based algorithm, Retinexformer, for low-light image enhancement.
- We formulate a one-stage Retinex-based low-light enhancement framework, ORF, that enjoys an easy one-stage training process and models the corruptions well.
- We design a new self-attention mechanism, IG-MSA, that utilizes the illumination information as a key clue to guide the modeling of long-range dependences.
- Quantitative and qualitative experiments show that our Retinexformer outperforms SOTA algorithms on seven datasets. The results of user study and low-light detection also suggest the practical values of our method.

2. Related Work

2.1. Low-light Image Enhancement

Plain Methods. Plain methods like histogram equalization [1, 7, 11, 40, 41] and Gamma Correction (GC) [18, 42, 52] directly amplify the low visibility and contrast of under-exposed images. Yet, these methods barely consider the illumination factors, making the enhanced images perceptually inconsistent with the real normal-light scenes.

Traditional Cognition Methods. Different from plain algorithms, conventional methods [14, 23, 24, 29, 49] bear the illumination factors into consideration. They rely on the Retinex theory and treat the reflectance component of the low-light image as a plausible solution of the enhanced result. For example, Guo *et al.* [17] propose to refine the initial estimated illumination map by imposing a structure prior on it. Wang *et al.* [49] design an algorithm NPE to preserve the naturalness of details during the enhancement of non-uniform illumination images. However, these methods naively assume that the low-light images are corruption-free, leading to severe noise and color distortion issues during the enhancement process. Besides, these methods rely on hand-crafted priors, usually requiring careful parameter tweaking and suffering from poor generalization ability.

Deep Learning Methods. With the rapid progress of deep learning, CNN [15, 16, 21, 22, 25, 34, 36, 38, 45, 48, 60, 65, 67] has been widely used in low-light image enhancement. For instance, Lore *et al.* [34] propose a stacked sparse denoising auto-encoder LLNet for joint low-light enhancement and noise suppression. Wei *et al.* [53] and follow-up works [64, 65] combine the Retinex decomposition with deep learning. However, these methods usually suffer from a tedious multi-stage training pipeline. Several CNNs are employed to learn or adjust different components of the Retinex model, respectively. Wang *et al.* [48] propose a one-stage Retinex-based CNN, dubbed DeepUPE, to directly predict the illumination map. Nonetheless, DeepUPE does not consider the corruption factors, leading to amplified noise and color distortion when lighting up under-exposed photos. In addition, these CNN-based methods also show limitations in capturing long-range dependencies.

2.2. Vision Transformer

The natural language processing model, Transformer, is proposed in [46] for machine translation. In recent years, Transformer and its variants have been applied in many computer vision tasks and achieved impressive results in high-level vision (*e.g.*, image classification [2, 4, 13], semantic segmentation [6, 54, 66], object detection [3, 12, 61], *etc.*) and low-level vision (*e.g.*, image restoration [5, 10, 30, 59], image synthesis [19, 20, 63], *etc.*). For example, Xu *et al.* [56] propose an SNR-aware CNN-Transformer hybrid network, SNR-Net, for low-light image enhancement. However, SNR-Net only employs a single global

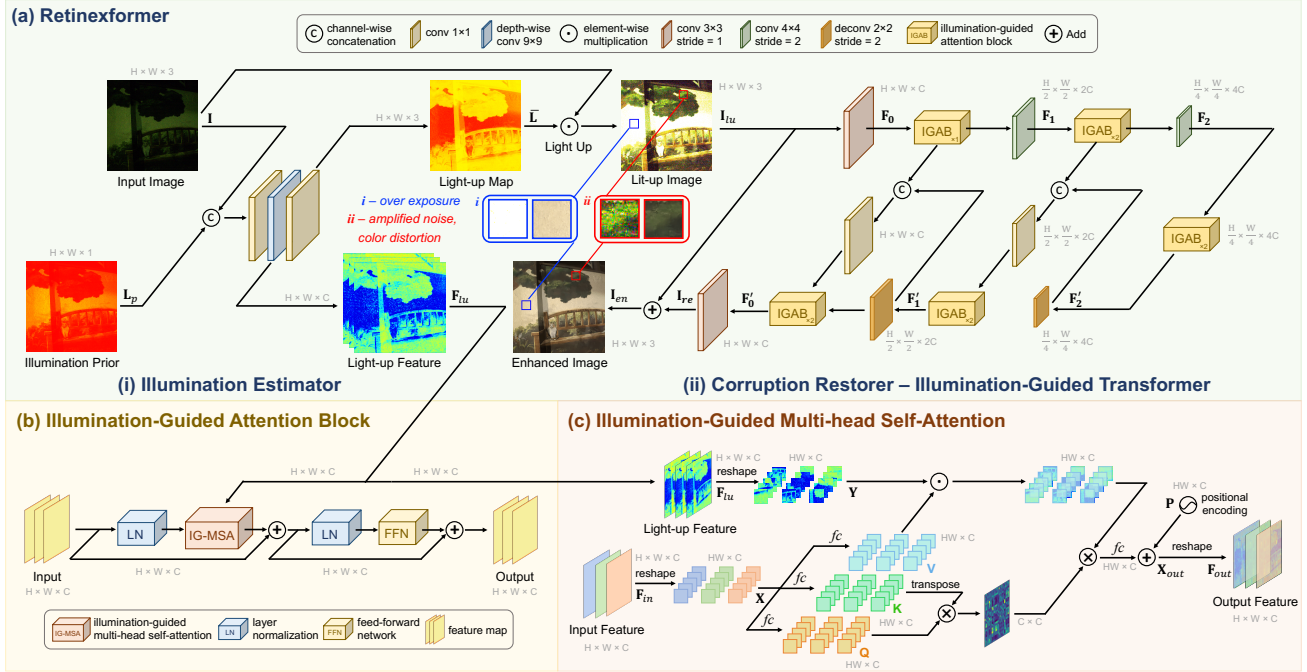


Figure 2. The overview of our method. (a) Retinexformer adopts the proposed ORF that consists of an illumination estimator (i) and a corruption restorer (ii) IGT. (b) The basic unit of IGT is IGAB, which is composed of two layer normalization (LN), an IG-MSA and a feed-forward network (FFN). (c) IG-MSA uses the illumination representations captured by ORF to direct the computation of self-attention.

Transformer layer at the lowest resolution of a U-shaped CNN due to the enormous computational costs of the vanilla global Transformer. The potential of Transformer has not been fully explored for low-light image enhancement.

3. Method

Fig. 2 illustrates the overall architecture of our method. As shown in Fig. 2 (a), our Retinexformer is based on our formulated One-stage Retinex-based Framework (ORF). ORF consists of an illumination estimator (i) and a corruption restorer (ii). We design an Illumination-Guided Transformer (IGT) to play the role of the corruption restorer. As depicted in Fig. 2 (b), the basic unit of IGT is Illumination-Guided Attention Block (IGAB), which is composed of two layer normalization (LN), an Illumination-Guided Multi-head Self-Attention (IG-MSA) module, and a feed-forward network (FFN). Fig. 2 (c) shows the details of IG-MSA.

3.1. One-stage Retinex-based Framework

According to the Retinex theory. A low-light image $\mathbf{I} \in \mathbb{R}^{H \times W \times 3}$ can be decomposed into a reflectance image $\mathbf{R} \in \mathbb{R}^{H \times W \times 3}$ and an illumination map $\mathbf{L} \in \mathbb{R}^{H \times W}$ as

$$\mathbf{I} = \mathbf{R} \odot \mathbf{L}, \quad (1)$$

where \odot denotes the element-wise multiplication. This Retinex model assumes \mathbf{I} is corruption-free, which is inconsistent with the real under-exposed scenes. We analyze that the corruptions mainly stem from two factors. Firstly, the high-ISO and long-exposure imaging settings of dark

scenes inevitably introduce noise and artifacts. Secondly, the light-up process may amplify the noise and artifacts and also cause under-/over-exposure and color distortion, as illustrated in the zoomed-in patch i and ii of Fig. 2 (a).

To model the corruptions, we reformulate Eq. (1) by introducing a perturbation term for \mathbf{R} and \mathbf{L} respectively, as

$$\begin{aligned} \mathbf{I} &= (\mathbf{R} + \hat{\mathbf{R}}) \odot (\mathbf{L} + \hat{\mathbf{L}}) \\ &= \mathbf{R} \odot \mathbf{L} + \mathbf{R} \odot \hat{\mathbf{L}} + \hat{\mathbf{R}} \odot (\mathbf{L} + \hat{\mathbf{L}}), \end{aligned} \quad (2)$$

where $\hat{\mathbf{R}} \in \mathbb{R}^{H \times W \times 3}$ and $\hat{\mathbf{L}} \in \mathbb{R}^{H \times W}$ denote the perturbations. Similar to [14, 17, 48], we regard \mathbf{R} as a well-exposed image. To light up \mathbf{I} , we element-wisely multiply the two sides of Eq. (2) by a light-up map $\bar{\mathbf{L}}$ such that $\bar{\mathbf{L}} \odot \mathbf{L} = \mathbf{1}$ as

$$\mathbf{I} \odot \bar{\mathbf{L}} = \mathbf{R} + \mathbf{R} \odot (\hat{\mathbf{L}} \odot \bar{\mathbf{L}}) + (\hat{\mathbf{R}} \odot (\mathbf{L} + \hat{\mathbf{L}})) \odot \bar{\mathbf{L}}, \quad (3)$$

where $\hat{\mathbf{R}} \odot (\mathbf{L} + \hat{\mathbf{L}})$ represents the noise and artifacts hidden in the dark scenes and are amplified by $\bar{\mathbf{L}}$. $\mathbf{R} \odot (\hat{\mathbf{L}} \odot \bar{\mathbf{L}})$ indicates the under-/over-exposure and color distortion caused by the light-up process. We simplify Eq. (3) as

$$\mathbf{I}_{lu} = \mathbf{I} \odot \bar{\mathbf{L}} = \mathbf{R} + \mathbf{C}, \quad (4)$$

where $\mathbf{I}_{lu} \in \mathbb{R}^{H \times W \times 3}$ represents the lit-up image and $\mathbf{C} \in \mathbb{R}^{H \times W \times 3}$ indicates the overall corruption term. Subsequently, we formulate our ORF as

$$(\mathbf{I}_{lu}, \mathbf{F}_{lu}) = \mathcal{E}(\mathbf{I}, \mathbf{L}_p), \quad \mathbf{I}_{en} = \mathcal{R}(\mathbf{I}_{lu}, \mathbf{F}_{lu}), \quad (5)$$

where \mathcal{E} denotes the illumination estimator and \mathcal{R} represents the corruption restorer. \mathcal{E} takes \mathbf{I} and its illumination prior map $\mathbf{L}_p \in \mathbb{R}^{H \times W}$ as inputs. $\mathbf{L}_p = \text{mean}_c(\mathbf{I})$ where

mean_c indicates the operation that calculates the mean values for each pixel along the channel dimension. \mathcal{E} outputs the lit-up image \mathbf{I}_{lu} and light-up feature $\mathbf{F}_{lu} \in \mathbb{R}^{H \times W \times C}$. Then \mathbf{I}_{lu} and \mathbf{F}_{lu} are fed into \mathcal{R} to restore the corruptions and produce the enhanced image $\mathbf{I}_{en} \in \mathbb{R}^{H \times W \times 3}$.

The architecture of \mathcal{E} is shown in Fig. 2 (a) (i). \mathcal{E} firstly uses a $conv1 \times 1$ (convolution with kernel size = 1) to fuse the concatenation of \mathbf{I} and \mathbf{L}_p . We notice that the well-exposed regions can provide semantic contextual information for under-exposed regions. Thus, a depth-wise separable $conv9 \times 9$ is adopted to model the interactions of regions with different lighting conditions to generate the light-up feature \mathbf{F}_{lu} . Then \mathcal{E} uses a $conv1 \times 1$ to aggregate \mathbf{F}_{lu} to produce the light-up map $\bar{\mathbf{L}} \in \mathbb{R}^{H \times W \times 3}$. We set $\bar{\mathbf{L}}$ as a three-channel RGB tensor instead of a single-channel one like [14, 17] to improve its representation capacity in simulating the nonlinearity across RGB channels for color enhancement. Then $\bar{\mathbf{L}}$ is used to light up \mathbf{I} in Eq. (3).

Discussion. (i) Different from previous Retinex-based deep learning methods [31, 48, 53, 64, 65], our ORF estimates $\bar{\mathbf{L}}$ instead of the illumination map \mathbf{L} because if ORF estimates \mathbf{L} , then the lit-up image will be obtained by an element-wise division (\mathbf{I}/\mathbf{L}). Computers are vulnerable to this operation. The values of tensors can be very small (sometimes even equal to 0). The division may easily cause the data overflow issue. Besides, small errors randomly generated by the computer will be amplified by this operation and lead to inaccurate estimation. Hence, modeling $\bar{\mathbf{L}}$ is more robust.

(ii) Previous Retinex-based deep learning methods mainly focus on suppressing the corruptions like noise on the reflectance image, *i.e.*, $\hat{\mathbf{R}}$ in Eq. (2). They overlook the estimation error on the illumination map, *i.e.*, $\hat{\mathbf{L}}$ in Eq. (2), thus easily leading to under-/over-exposure and color distortion during the light up process. In contrast, our ORF considers all these corruptions and employs \mathcal{R} to restore them all.

3.2. Illumination-Guided Transformer

Previous deep learning methods mainly rely on CNNs, showing limitations in capturing long-range dependencies. Some CNN-Transformer hybrid works like SNR-Net [56] only employ a global Transformer layer at the lowest resolution of a U-shaped CNN due to the enormous computational complexity of global multi-head self-attention (MSA). The potential of Transformer has not been fully explored. To fill this gap, we design an Illumination-Guided Transformer (IGT) to play the role of the corruption restorer \mathcal{R} in Eq. (5).

Network Structure. As illustrated in Fig. 2 (a) (ii), IGT adopts a three-scale U-shaped architecture [44]. The input of IGT is the lit-up image \mathbf{I}_{lu} . In the downsampling branch, \mathbf{I}_{lu} undergoes a $conv3 \times 3$, an IGAB, a strided $conv4 \times 4$ (for downsampling the features), two IGABs, and a strided $conv4 \times 4$ to generate hierarchical features $\mathbf{F}_i \in \mathbb{R}^{\frac{H}{2^i} \times \frac{W}{2^i} \times 2^i C}$ where $i = 0, 1, 2$. Then \mathbf{F}_2 passes through two

IGABs. Subsequently, a symmetrical structure is designed as the upsampling branch. The $deconv2 \times 2$ with stride = 2 is exploited to upscale the features. Skip connections are used to alleviate the information loss caused by the downsampling branch. The upsampling branch outputs a residual image $\mathbf{I}_{re} \in \mathbb{R}^{H \times W \times 3}$. Then the enhanced image \mathbf{I}_{en} is derived by the sum of \mathbf{I}_{lu} and \mathbf{I}_{re} , *i.e.*, $\mathbf{I}_{en} = \mathbf{I}_{lu} + \mathbf{I}_{re}$.

IG-MSA. As illustrated in Fig. 2 (c), the light-up feature $\mathbf{F}_{lu} \in \mathbb{R}^{H \times W \times C}$ estimated by \mathcal{E} is fed into each IG-MSA of IGT. Please note that Fig. 2 (c) depicts IG-MSA for the largest scale. For smaller scales, $conv4 \times 4$ layers with stride = 2 are used to downscale \mathbf{F}_{lu} to match the spatial size, which is omitted in this figure. As aforementioned, the non-trivial computational cost of global MSA limits the application of Transformer in low-light image enhancement. To tackle this issue, IG-MSA treats a single-channel feature map as a token and then computes the self-attention.

Firstly, the input feature $\mathbf{F}_{in} \in \mathbb{R}^{H \times W \times C}$ is reshaped into tokens $\mathbf{X} \in \mathbb{R}^{HW \times C}$. Then \mathbf{X} is split into k heads:

$$\mathbf{X} = [\mathbf{X}_1, \mathbf{X}_2, \dots, \mathbf{X}_k], \quad (6)$$

where $\mathbf{X}_i \in \mathbb{R}^{HW \times d_k}$, $d_k = \frac{C}{k}$, and $i = 1, 2, \dots, k$. Note that Fig. 2 (c) shows the situation with $k = 1$ and omits some details for simplification. For each *head* _{i} , three fully connected (*fc*) layers without *bias* are used to linearly project \mathbf{X}_i into *query* elements $\mathbf{Q}_i \in \mathbb{R}^{HW \times d_k}$, *key* elements $\mathbf{K}_i \in \mathbb{R}^{HW \times d_k}$, and *value* elements $\mathbf{V}_i \in \mathbb{R}^{HW \times d_k}$ as

$$\mathbf{Q}_i = \mathbf{X}_i \mathbf{W}_{\mathbf{Q}_i}^T, \quad \mathbf{K}_i = \mathbf{X}_i \mathbf{W}_{\mathbf{K}_i}^T, \quad \mathbf{V}_i = \mathbf{X}_i \mathbf{W}_{\mathbf{V}_i}^T, \quad (7)$$

where $\mathbf{W}_{\mathbf{Q}_i}$, $\mathbf{W}_{\mathbf{K}_i}$, and $\mathbf{W}_{\mathbf{V}_i} \in \mathbb{R}^{d_k \times d_k}$ represent the learnable parameters of the *fc* layers and T denotes the matrix transpose. We notice that different regions of the same image may have different lighting conditions. Dark regions usually have severer corruptions and are more difficult to restore. Regions with better lighting conditions can provide semantic contextual representations to help enhance the dark regions. Thus, we use the light-up feature \mathbf{F}_{lu} encoding illumination information and interactions of regions with different lighting conditions to direct the computation of self-attention. To align with the shape of \mathbf{X} , we also reshape \mathbf{F}_{lu} into $\mathbf{Y} \in \mathbb{R}^{HW \times C}$ and split it into k heads:

$$\mathbf{Y} = [\mathbf{Y}_1, \mathbf{Y}_2, \dots, \mathbf{Y}_k], \quad (8)$$

where $\mathbf{Y}_i \in \mathbb{R}^{HW \times d_k}$, $i = 1, 2, \dots, k$. Then the self-attention for each *head* _{i} is formulated as

$$\text{Attention}(\mathbf{Q}_i, \mathbf{K}_i, \mathbf{V}_i, \mathbf{Y}_i) = (\mathbf{Y}_i \odot \mathbf{V}_i) \text{softmax}\left(\frac{\mathbf{K}_i^T \mathbf{Q}_i}{\alpha_i}\right), \quad (9)$$

where $\alpha_i \in \mathbb{R}^1$ is a learnable parameter that adaptively scales the matrix multiplication. Subsequently, k heads are concatenated to pass through an *fc* layer and then plus a positional encoding $\mathbf{P} \in \mathbb{R}^{HW \times C}$ (learnable parameters) to produce the output tokens $\mathbf{X}_{out} \in \mathbb{R}^{HW \times C}$. Finally, we reshape \mathbf{X}_{out} to derive the output feature $\mathbf{F}_{out} \in \mathbb{R}^{H \times W \times C}$.

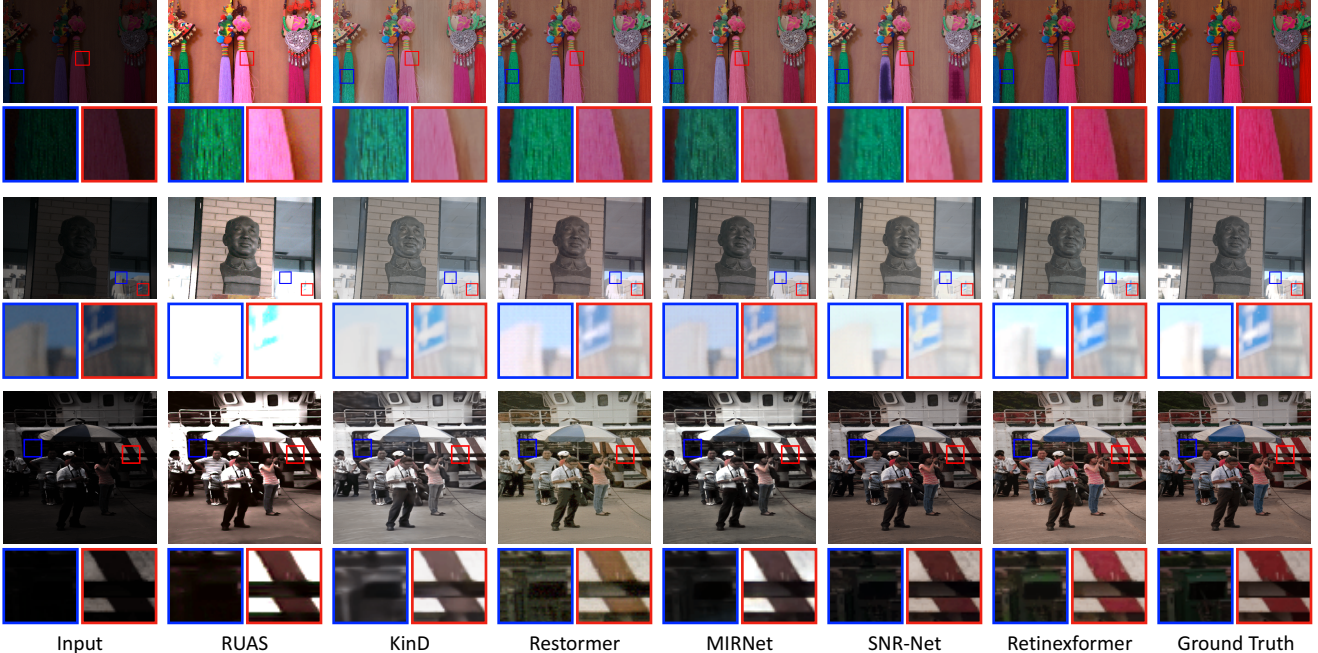


Figure 3. Visual results on LOL-v1 [53] (top), LOL-v2 [58]-real (middle), and LOL-v2-synthetic (bottom). Other methods cause under-/over-exposure, or color distortion, or blurry textures. While Retinexformer can effectively enhance the visibility and preserve the color.

Complexity Analysis. We analyze that the computational complexity of our IG-MSA mainly comes from the k computations of the two matrix multiplication in Eq. (9), *i.e.*, $\mathbb{R}^{d_k \times HW} \times \mathbb{R}^{HW \times d_k}$ and $\mathbb{R}^{HW \times d_k} \times \mathbb{R}^{d_k \times d_k}$. Therefore, the complexity $\mathcal{O}(\text{IG-MSA})$ can be formulated as

$$\begin{aligned} \mathcal{O}(\text{IG-MSA}) &= k \cdot [d_k \cdot (d_k \cdot HW) + HW \cdot (d_k \cdot d_k)], \\ &= 2HWkd_k^2 = 2HWk\left(\frac{C}{k}\right)^2 = \frac{2HWC^2}{k}. \end{aligned} \quad (10)$$

While the complexity of the global MSA (G-MSA) used by some previous CNN-Transformer methods like SNR-Net is

$$\mathcal{O}(\text{G-MSA}) = 2(HW)^2C. \quad (11)$$

Compare Eq. (10) with Eq. (11). $\mathcal{O}(\text{G-MSA})$ is quadratic to the input spatial size (HW). This burden is expensive and limits the application of Transformer for low-light image enhancement. Therefore, previous CNN-Transformer hybrid algorithms only employ a G-MSA layer at the lowest spatial resolution of a U-shaped CNN to save the computational costs. In contrast, $\mathcal{O}(\text{IG-MSA})$ is linear to the spatial size. This much lower computational complexity enables our IG-MSA to be plugged into each basic unit IGAB of the network. By this means, the potential of Transformer for low-light image enhancement can be further explored.

4. Experiment

4.1. Datasets and Implementation Details

We evaluate our method on LOL (v1 [53] and v2 [58]), SID [8], SMID [9], and SDSD [47] (indoor and outdoor).

LOL. The LOL dataset has two versions: v1 and v2. LOL-v1 provides 485 low-/normal-light image pairs for training and 15 image pairs for testing. Each pair contains a low-light image and its corresponding well-exposed reference image. LOL-v2 is divided into two subsets, *i.e.*, LOL-v2-real and LOL-v2-synthetic. The train set of LOL-v2-real includes 689 low-/normal-light image pairs and the test set contains 100 pairs. Most low-light images are captured from a variety of scenes by changing the ISO and exposure time, while other parameters are fixed. LOL-v2-synthetic is created by analyzing the illumination distribution of low-light images and then synthesizing from RAW images.

SID. The subset of SID dataset captured by the Sony $\alpha 7S$ II camera is adopted for evaluation. There are 2697 short-/long-exposure RAW image pairs. The low-/normal-light RGB images are obtained by using the same in-camera signal processing of SID [8] to transfer the RAW images to RGB domain. 2099 low-/normal-light image pairs are used for training and 598 image pairs are selected for testing.

SMID. The SMID benchmark collects 20809 short-/long-exposure RAW image pairs. We transfer the RAW data to low-/normal-light RGB image pairs. 15763 pairs are used for training and the left pairs are adopted for testing.

SDSD. The static version of the SDSD dataset is adopted for evaluation. It is captured by a Canon EOS 6D Mark II camera with an ND filter. The SDSD dataset contains two subsets, *i.e.*, SDSD-indoor and SDSD-outdoor. SDSD-indoor includes 62 low-/normal-light video pairs for training and 6 pairs for testing. SDSD-outdoor contains 116 low-/normal-light video pairs for training and 10 video pairs for testing.

Methods	Complexity		LOL-v1		LOL-v2-real		LOL-v2-syn		SID		SMID		SDSD-in		SDSD-out	
	FLOPS (G)	Params (M)	PSNR	SSIM	PSNR	SSIM	PSNR	SSIM	PSNR	SSIM	PSNR	SSIM	PSNR	SSIM	PSNR	SSIM
SID [8]	13.73	7.76	14.35	0.436	13.24	0.442	15.04	0.610	16.97	0.591	24.78	0.718	23.29	0.703	24.90	0.693
3DLUT [62]	0.075	0.59	14.35	0.445	17.59	0.721	18.04	0.800	20.11	0.592	23.86	0.678	21.66	0.655	21.89	0.649
DeepUPE [48]	21.10	1.02	14.38	0.446	13.27	0.452	15.08	0.623	17.01	0.604	23.91	0.690	21.70	0.662	21.94	0.698
RF [27]	46.23	21.54	15.23	0.452	14.05	0.458	15.97	0.632	16.44	0.596	23.11	0.681	20.97	0.655	21.21	0.689
DeepLPF [38]	5.86	1.77	15.28	0.473	14.10	0.480	16.02	0.587	18.07	0.600	24.36	0.688	22.21	0.664	22.76	0.658
IPT [10]	6887	115.31	16.27	0.504	19.80	0.813	18.30	0.811	20.53	0.561	27.03	0.783	26.11	0.831	27.55	0.850
UFormer [51]	12.00	5.29	16.36	0.771	18.82	0.771	19.66	0.871	18.54	0.577	27.20	0.792	23.17	0.859	23.85	0.748
RetinexNet [53]	587.47	0.84	16.77	0.560	15.47	0.567	17.13	0.798	16.48	0.578	22.83	0.684	20.84	0.617	20.96	0.629
Sparse [58]	53.26	2.33	17.20	0.640	20.06	0.816	22.05	0.905	18.68	0.606	25.48	0.766	23.25	0.863	25.28	0.804
EnGAN [21]	61.01	114.35	17.48	0.650	18.23	0.617	16.57	0.734	17.23	0.543	22.62	0.674	20.02	0.604	20.10	0.616
RUAS [31]	0.83	0.003	18.23	0.720	18.37	0.723	16.55	0.652	18.44	0.581	25.88	0.744	23.17	0.696	23.84	0.743
FIDE [55]	28.51	8.62	18.27	0.665	16.85	0.678	15.20	0.612	18.34	0.578	24.42	0.692	22.41	0.659	22.20	0.629
DRBN [57]	48.61	5.27	20.13	0.830	20.29	0.831	23.22	0.927	19.02	0.577	26.60	0.781	24.08	0.868	25.77	0.841
KinD [65]	34.99	8.02	20.86	0.790	14.74	0.641	13.29	0.578	18.02	0.583	22.18	0.634	21.95	0.672	21.97	0.654
Restormer [59]	144.25	26.13	22.43	0.823	19.94	0.827	21.41	0.830	22.27	0.649	26.97	0.758	25.67	0.827	24.79	0.802
MIRNet [60]	785	31.76	24.14	0.830	20.02	0.820	21.94	0.876	20.84	0.605	25.66	0.762	24.38	0.864	27.13	0.837
SNR-Net [56]	26.35	4.01	24.61	0.842	21.48	0.849	24.14	0.928	22.87	0.625	28.49	0.805	29.44	0.894	28.66	0.866
Retinexformer	15.57	1.61	25.16	0.845	22.80	0.840	25.67	0.939	24.44	0.680	29.15	0.815	29.77	0.896	29.84	0.877

Table 1. Quantitative comparisons on LOL (v1 [53] and v2 [58]), SID [8], SMID [9], and SDSD [47] (indoor and outdoor) datasets. The highest result is in red color while the second highest result is in blue color. Our Retinexformer significantly outperforms SOTA algorithms.

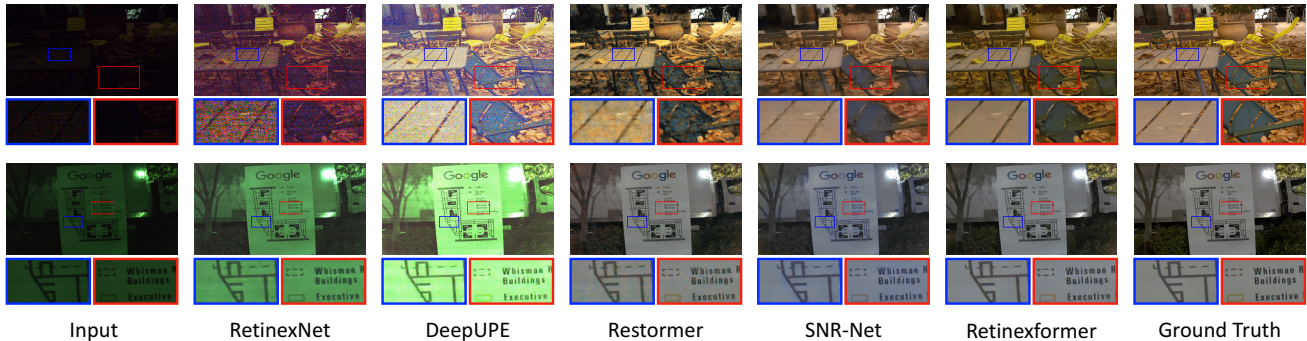


Figure 4. Visual results on SID [8] (top) and SMID [9] (bottom). Previous methods either collapse by noise, or distort color, or produce blurry and under-/over-exposed images. While our algorithm can effectively remove the noise and reconstruct well-exposed image details.

Implementation Details. We implement Retinexformer by PyTorch [39]. The model is trained with the Adam [26] optimizer ($\beta_1 = 0.9$ and $\beta_2 = 0.999$) for 2.5×10^5 iterations. The learning rate is initially set to 2×10^{-4} and then steadily decreased to 1×10^{-6} by the cosine annealing scheme [35] during the training process. Patches at the size of 128×128 are randomly cropped from the low-/normal-light image pairs as training samples. The batch size is 8. The training data is augmented with random rotation and flipping. The training objective is to minimize the mean absolute error (MAE) between the lit-up image and enhanced image. We adopt the peak signal-to-noise ratio (PSNR) and structural similarity (SSIM) [50] as the evaluation metrics.

4.2. Low-light Image Enhancement

Quantitative Results. We compare our method with a wide range of SOTA enhancement algorithms. The PSNR and SSIM results are reported in Tab. 1. Our Retinexformer significantly outperforms SOTA methods on the seven datasets while requiring moderate computational and memory costs.

When compared with the recent best method SNR-Net,

our Retinexformer achieves 0.55, 1.32, 1.53, 1.57, 0.66, 0.33, and 1.18 dB improvements on LOL-v1, LOL-v2-real, LOL-v2-synthetic, SID, SMID, SDSD-indoor, and SDSD-outdoor datasets. However, our Retinexformer only costs 40% (1.61 / 4.01) Params and 59% (15.57 / 26.35) FLOPS.

When compared with SOTA Retinex-based deep learning methods (including DeepUPE [48], RetinexNet [53], RUAS [31], and KinD [65]), our Retinexformer yields 4.30, 4.43, 8.54, 6.00, 3.27, 6.60, and 6.00 dB improvements on the seven benchmarks. Especially on SID and SDSD datasets that are severely corrupted by noise and artifacts, the improvements are **over 6 dB**, as plotted in Fig. 1.

When compared with SOTA Transformer-based image restoration algorithms (including IPT [10], Uformer [51], and Restormer [59]), our Retinexformer gains by 2.73, 2.86, 4.26, 2.17, 1.95, 3.66, and 2.29 dB on the seven datasets. Nonetheless, Retinexformer requires only 1.4% and 6.2% Params, 0.2% and 10.9% FLOPS of IPT and Restormer.

All these results clearly suggest the outstanding effectiveness and efficiency advantage of our Retinexformer.

Methods	L-v1	L-v2-R	L-v2-S	SID	SMID	SD-in	SD-out	Mean
EnGAN [21]	2.43	1.39	2.13	1.04	2.78	1.83	1.87	1.92
RetinexNet [53]	2.17	1.91	1.13	1.09	2.35	3.96	3.74	2.34
DRBN [57]	2.70	2.26	3.65	1.96	2.22	2.78	2.91	2.64
FIDE [55]	2.87	2.52	3.48	2.22	2.57	3.04	2.96	2.81
Kind [65]	2.65	2.48	3.17	1.87	3.04	3.43	3.39	2.86
MIRNet [60]	2.96	3.57	3.61	2.35	2.09	2.91	3.09	2.94
Restormer [59]	3.04	3.48	3.39	2.43	3.17	2.48	2.70	2.96
RUAS [31]	3.83	3.22	2.74	2.26	3.48	3.39	3.04	3.14
SNR-Net [56]	3.13	3.83	3.57	3.04	3.30	2.74	3.17	3.25
Retinexformer	3.61	4.17	3.78	3.39	3.87	3.65	3.91	3.77

Methods	Bicycle	Boat	Bottle	Bus	Car	Cat	Chair	Cup	Dog	Motor	People	Table	Mean
MIRNet [60]	71.8	63.8	62.9	81.4	71.1	58.8	58.9	61.3	63.1	52.0	68.8	45.5	63.6
RetinexNet [53]	73.8	62.8	64.8	84.9	80.8	53.4	57.2	68.3	61.5	51.3	65.9	43.1	64.0
RUAS [31]	72.0	62.2	65.2	72.9	78.1	57.3	62.4	61.8	60.2	61.5	69.4	46.8	64.2
Restormer [59]	76.2	65.1	64.2	84.0	76.3	59.2	53.0	58.7	66.1	62.9	68.6	45.0	64.9
Kind [65]	72.2	66.5	58.9	83.7	74.5	55.4	61.7	61.3	63.8	63.0	70.5	47.8	65.0
ZeroDCE [16]	75.8	66.5	65.6	84.9	77.2	56.3	53.8	59.0	63.5	64.0	68.3	46.3	65.1
SNR-Net [56]	75.3	64.4	63.6	85.3	77.5	59.1	54.1	59.6	66.3	65.2	69.1	44.6	65.3
SCI [37]	74.6	65.3	65.8	85.4	76.3	59.4	57.1	60.5	65.6	63.9	69.1	45.9	65.6
Retinexformer	76.3	66.7	65.9	84.7	77.6	61.2	53.5	60.7	67.5	63.4	69.5	46.0	66.1

(a) User study scores on the seven benchmarks.

(b) Low-light detection results on ExDark [33] enhanced by different algorithms.

Table 2. (a) compares the human perception quality of various low-light enhancement algorithms. (b) compares the preprocessing effects of different methods on high-level vision understanding. The highest results are in red color and the second highest results are in blue color.

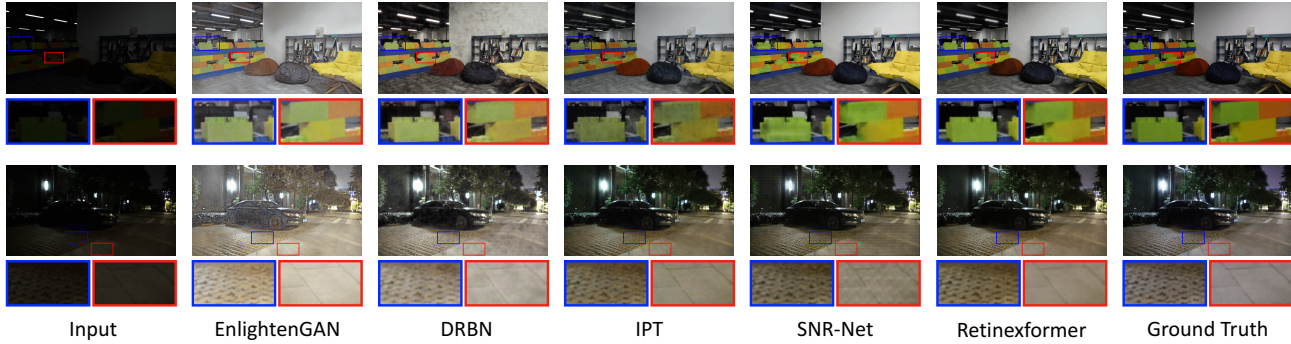


Figure 5. Visual result on SDDS [47]-indoor (top) and outdoor (bottom). Other algorithms either generate over-exposed and noisy images, or introduce black spot corruptions and unnatural artifacts. While Retinexformer can restore well-exposed structural contents and textures.

Qualitative Results. The visual results of Retinexformer and SOTA algorithms on the seven benchmarks are shown in Fig. 3, 4, and 5. Please zoom in for a better view. Previous methods either cause color distortion like RUAS in Fig. 3, or contain over-/under-exposed regions and fail to suppress the noise like RetinexNet and DeepUPE in Fig. 4, or generate blurry images like Restormer and SNR-Net in Fig. 4, or introduce black spots and unnatural artifacts like DRBN [57] and SNR-Net in Fig. 5. In contrast, our Retinexformer can effectively enhance the poor visibility and low contrast, reliably remove the noise without introducing spots and artifacts, and robustly preserve the color.

User Study Score. We conduct a user study to quantify the human subjective visual perception quality of the enhanced low-light images from the seven datasets. 23 human subjects are invited to score the visual quality of the enhanced results, independently. These testers are told to observe the results from: (i) whether the results contain under-/over-exposed regions, (ii) whether the results contain color distortion, and (iii) whether the results are corrupted by noise or artifacts. The scores range from 1 (worst) to 5 (best). For each low-light image, we display it and the results enhanced by various algorithms but without their names to the human testers. There are 156 testing images in total. The user study scores are reported in Tab. 2a. Our Retinexformer achieves the highest score on average. Besides, our results are most favored by the human subjects on LOL-v2-real (L-v2-R), LOL-v2-synthetic (L-v2-S), SID, SMID, and

SDDS-outdoor (SD-out) datasets and second most favored on LOL-v1 (L-v1) and SDDS-indoor (SD-in) benchmarks.

4.3. Low-light Object Detection

Experiment Settings. We conduct low-light object detection experiments on the ExDark [33] dataset to compare the preprocessing effects of different enhancement algorithms for high-level vision understanding. The ExDark dataset consists of 7363 under-exposed images annotated with 12 object category bounding boxes. 5890 images are selected for training while the left 1473 images are used for testing. YOLO-v3 [43] is employed as the detector and trained from scratch. Different low-light enhancement methods serve as the preprocessing modules with fixed parameters.

Quantitative Results. The average precision (AP) scores are listed in Tab. 2b. Our Retinexformer achieves the highest result on average, 66.1 AP, which is 0.5 AP higher than the recent best self-supervised method SCI [37] and 0.8 AP higher than the recent best fully-supervised method SNR-Net [56]. Besides, Retinexformer yields the best results on five object categories: bicycle, boat, bottle, cat, and dog.

Qualitative Results. Fig. 6 depicts the visual comparisons of detection results. The detector easily misses some target objects or predicts inaccurate locations on the images enhanced by previous algorithms. In contrast, the detector can reliably predict well-placed bounding boxes to cover all the desired objects on the image enhanced by our Retinexformer. These results demonstrate the superiority of the proposed method in benefiting high-level vision understanding.

Baseline-1	ORF	IG-MSA	PSNR	SSIM	Params (M)	FLOPS (G)	Method	$I_{lu} = \mathbf{I}$	$I_{lu} = \mathbf{I}/\mathbf{L}$	$I_{lu} = \mathbf{I} \odot \bar{\mathbf{L}}$	$+F_{lu}$	Method	Baseline-2	G-MSA	W-MSA	IG-MSA
✓			26.47	0.843	1.01	9.18	PSNR	28.86	28.97	29.26	29.84	PSNR	27.92	28.43	28.65	29.84
	✓		27.92	0.857	1.27	11.37	SSIM	0.868	0.868	0.870	0.877	SSIM	0.857	0.841	0.845	0.877
		✓	28.86	0.868	1.34	13.38	Params (M)	1.34	1.61	1.61	1.61	Params (M)	1.27	1.61	1.61	1.61
✓	✓	✓	29.84	0.877	1.61	15.57	FLOPS (G)	13.38	14.01	14.01	15.57	FLOPS (G)	11.37	17.65	16.43	15.57

(a) Break-down ablation towards higher performance. (b) Ablation of the proposed ORF. (c) Ablation of self-attention schemes.

TABLE 3. We conduct ablation study on the SDSO [47]-outdoor dataset. PSNR, SSIM, Params, and FLOPS (size = 256×256) are reported.

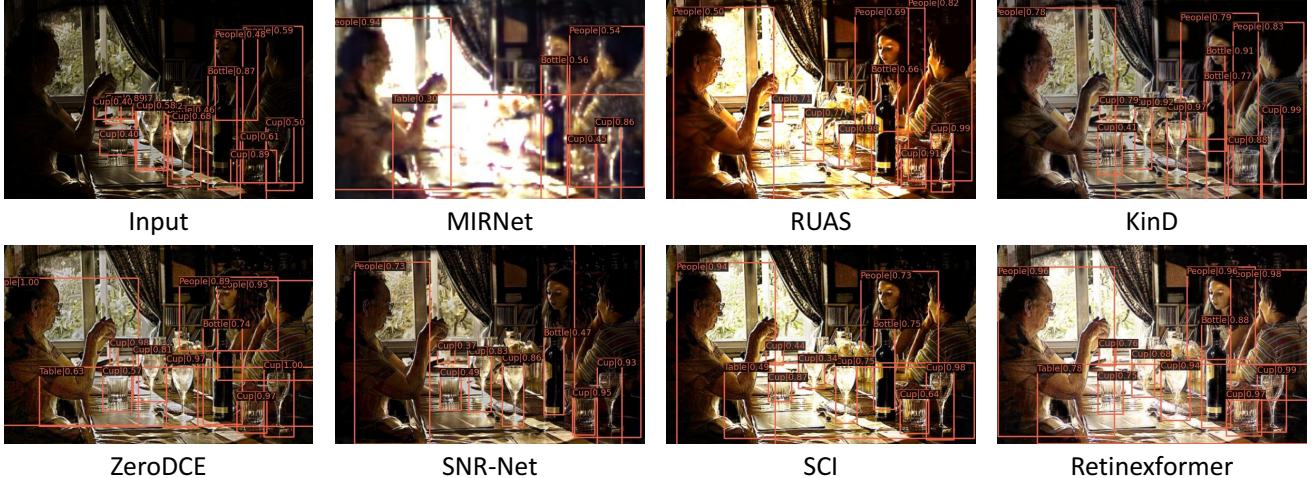


Figure 6. Visual comparisons of enhancement-based low-light object detection on the ExDark [33] dataset. Different enhancement methods serve as the preprocessing modules to enhance the low-light image before detection. Please zoom in for better visualization performance.

4.4. Ablation Study

We conduct ablation study on the SDSO-outdoor dataset for the good convergence and stable performance of Retinexformer on it. The results are reported in Tab. 3.

Break-down Ablation. We conduct a break-down ablation to study the effect of each component towards higher performance, as shown in Tab. 3a. Baseline-1 is derived by removing ORF and IG-MSA from Retinexformer. When we respectively apply ORF and IG-MSA, baseline-1 achieves 1.45 and 2.39 dB improvements. When jointly exploiting the two techniques, baseline-1 gains by 3.37 dB. This evidence suggests the effectiveness of our ORF and IG-MSA.

One-stage Retinex-based Framework. We conduct an ablation to study ORF. The results are listed in Tab. 3b. We first remove ORF from Retinexformer and set the input of \mathcal{R} as $I_{lu} = \mathbf{I}$. The model yields 28.86 dB. Then we apply ORF but set \mathcal{E} to estimate the illumination map \mathbf{L} . The input of \mathcal{R} is \mathbf{I}/\mathbf{L} where $/$ indicates the element-wise division. To avoid exceptions thrown by computer, we add \mathbf{L} with a small constant $\epsilon = 1 \times 10^{-4}$. Yet, as analyzed in Sec. 3.1, the computer is vulnerable to the division of small values. Thus, the model obtains a limited improvement of 0.11 dB. To tackle this issue, we estimate the light-up map $\bar{\mathbf{L}}$ and set the input of \mathcal{R} as $I_{lu} = \mathbf{I} \odot \bar{\mathbf{L}}$. The model gains by 0.40 dB. After using F_{lu} to direct \mathcal{R} , the model continues to achieve an improvement of 0.58 dB in PSNR and 0.007 in SSIM.

Self-Attention Scheme. We conduct an ablation to study the effect of the self-attention scheme. The results are re-

ported in Tab. 3c. Baseline-2 is obtained by removing IG-MSA from Retinexformer. For fair comparison, we plug the global MSA (G-MSA) used by previous CNN-Transformer hybrid methods into each basic unit of \mathcal{R} . The input feature maps of G-MSA are downscaled into $\frac{1}{4}$ size to avoid out of memory. We also compare our IG-MSA with local window-based MSA (W-MSA) proposed by Swin Transformer [32]. As listed in Tab. 3c, our IG-MSA surpasses G-MSA and W-MSA by 1.41 and 1.34 dB while costing 2.08G and 0.86G FLOPS less. These results demonstrate the cost-effectiveness advantage of the proposed IG-MSA.

5. Conclusion

In this paper, we propose a novel Transformer-based method, Retinexformer, for low-light image enhancement. We start from the Retinex theory. By analyzing the corruptions hidden in the under-exposed scenes and caused by the light-up process, we introduce perturbation terms into the original Retinex model and formulate a new Retinex-based framework, ORF. Then we design an IGT that utilizes the illumination information captured by ORF to direct the modeling of long-range dependences and interactions of regions with different lighting conditions. Finally, our Retinexformer is derived by plugging IGT into ORF. Extensive quantitative and qualitative experiments show that our Retinexformer dramatically outperforms SOTA methods on seven datasets. The results of user study and low-light detection also demonstrate the practical values of our method.

References

- [1] Mohammad Abdullah-Al-Wadud, Md Hasanul Kabir, M Ali Akber Dewan, and Oksam Chae. A dynamic histogram equalization for image contrast enhancement. *IEEE Transactions on Consumer Electronics*, 2007.
- [2] Alaaeldin Ali, Hugo Touvron, Mathilde Caron, Piotr Bojanowski, Matthijs Douze, Armand Joulin, Ivan Laptev, Natalia Neverova, Gabriel Synnaeve, Jakob Verbeek, et al. Xcit: Cross-covariance image transformers. In *NeurIPS*, 2021.
- [3] Nicolas arion, Francisco Massa, Gabriel Synnaeve, Nicolas Usunier, Alexander Kirillov, and Sergey Zagoruyko. End-to-end object detection with transformers. In *ECCV*, 2020.
- [4] Anurag Arnab, Mostafa Dehghani, Georg Heigold, Chen Sun, Mario Lučić, and Cordelia Schmid. Vivit: A video vision transformer. In *ICCV*, 2021.
- [5] Yuanhao Cai, Jing Lin, Haoqian Wang, Xin Yuan, Henghui Ding, Yulun Zhang, Radu Timofte, and Luc Van Gool. Degradation-aware unfolding half-shuffle transformer for spectral compressive imaging. In *NeurIPS*, 2022.
- [6] Hu Cao, Yueyue Wang, Joy Chen, Dongsheng Jiang, Xiaopeng Zhang, Qi Tian, and Manning Wang. Swin-unet: Unet-like pure transformer for medical image segmentation. In *ECCVW*, 2022.
- [7] Turgay Celik and Tardi Tjahjadi. Contextual and variational contrast enhancement. *TIP*, 2011.
- [8] Chen Chen, Qifeng Chen, Minh N Do, and Vladlen Koltun. Seeing motion in the dark. In *ICCV*, 2019.
- [9] Chen Chen, Qifeng Chen, Jia Xu, and Vladlen Koltun. Learning to see in the dark. In *CVPR*, 2018.
- [10] Hanting Chen, Yunhe Wang, Tianyu Guo, Chang Xu, Yiping Deng, Zhenhua Liu, Siwei Ma, Chunjing Xu, Chao Xu, and Wen Gao. Pre-trained image processing transformer. In *CVPR*, 2021.
- [11] Heng-Da Cheng and XJ Shi. A simple and effective histogram equalization approach to image enhancement. *Digital signal processing*, 2004.
- [12] Xiyang Dai, Yinpeng Chen, Jianwei Yang, Pengchuan Zhang, Lu Yuan, and Lei Zhang. Dynamic detr: End-to-end object detection with dynamic attention. In *ICCV*, 2021.
- [13] Alexey Dosovitskiy, Lucas Beyer, Alexander Kolesnikov, Dirk Weissenborn, Xiaohua Zhai, Thomas Unterthiner, Mostafa Dehghani, Matthias Minderer, Georg Heigold, Sylvain Gelly, Jakob Uszkoreit, and Neil Houlsby. An image is worth 16x16 words: Transformers for image recognition at scale. In *ICLR*, 2021.
- [14] Xueyang Fu, Delu Zeng, Yue Huang, Xiao-Ping Zhang, and Xinghao Ding. A weighted variational model for simultaneous reflectance and illumination estimation. In *CVPR*, 2016.
- [15] Ying Fu, Yang Hong, Linwei Chen, and Shaodi You. Legan: unsupervised low-light image enhancement network using attention module and identity invariant loss. *Knowledge-Based Systems*, 2022.
- [16] Chunle Guo, Chongyi Li, Jichang Guo, Chen Change Loy, Junhui Hou, Sam Kwong, and Runmin Cong. Zero-reference deep curve estimation for low-light image enhancement. In *CVPR*, 2020.
- [17] Xiaojie Guo, Yu Li, and Haibin Ling. Lime: Low-light image enhancement via illumination map estimation. *TIP*, 2016.
- [18] Shih-Chia Huang, Fan-Chieh Cheng, and Yi-Sheng Chiu. Efficient contrast enhancement using adaptive gamma correction with weighting distribution. *TIP*, 2012.
- [19] Drew A Hudson and Larry Zitnick. Generative adversarial transformers. In *ICML*, 2021.
- [20] Yifan Jiang, Shiyu Chang, and Zhangyang Wang. Transgan: Two pure transformers can make one strong gan, and that can scale up. In *NeurIPS*, 2021.
- [21] Yifan Jiang, Xinyu Gong, Ding Liu, Yu Cheng, Chen Fang, Xiaohui Shen, Jianchao Yang, Pan Zhou, and Zhangyang Wang. Enlightengan: Deep light enhancement without paired supervision. *TIP*, 2021.
- [22] Yeying Jin, Wenhan Yang, and Robby T Tan. Unsupervised night image enhancement: When layer decomposition meets light-effects suppression. In *ECCV*, 2022.
- [23] Daniel J Jobson, Zia-ur Rahman, and Glenn A Woodell. A multiscale retinex for bridging the gap between color images and the human observation of scenes. *TIP*, 1997.
- [24] Daniel J Jobson, Zia-ur Rahman, and Glenn A Woodell. Properties and performance of a center/surround retinex. *TIP*, 1997.
- [25] Hanul Kim, Su-Min Choi, Chang-Su Kim, and Yeong Jun Koh. Representative color transform for image enhancement. In *ICCV*, 2021.
- [26] Diederik P. Kingma and Jimmy Lei Ba. Adam: A method for stochastic optimization. In *ICLR*, 2015.
- [27] Satoshi Kosugi and Toshihiko Yamasaki. Unpaired image enhancement featuring reinforcement-learning-controlled image editing software. In *AAAI*, 2020.
- [28] Edwin H Land. The retinex theory of color vision. *Scientific american*, 1977.
- [29] Mading Li, Jiaying Liu, Wenhan Yang, Xiaoyan Sun, and Zongming Guo. Structure-revealing low-light image enhancement via robust retinex model. *TIP*, 2018.
- [30] Jingyun Liang, Jiezhong Cao, Guolei Sun, Kai Zhang, Luc Van Gool, and Radu Timofte. Swinir: Image restoration using swin transformer. In *ICCVW*, 2021.
- [31] Risheng Liu, Long Ma, Jiaao Zhang, Xin Fan, and Zhongxuan Luo. Retinex-inspired unrolling with cooperative prior architecture search for low-light image enhancement. In *CVPR*, 2021.
- [32] Ze Liu, Yutong Lin, Yue Cao, Han Hu, Yixuan Wei, Zheng Zhang, Stephen Lin, and Baining Guo. Swin transformer: Hierarchical vision transformer using shifted windows. In *ICCV*, 2021.
- [33] Yuen Peng Loh and Chee Seng Chan. Getting to know low-light images with the exclusively dark dataset. *Computer Vision and Image Understanding*, 2019.
- [34] Kin Gwn Lore, Adedotun Akintayo, and Soumik Sarkar. Llnet: A deep autoencoder approach to natural low-light image enhancement. *Pattern Recognition*, 2017.
- [35] Ilya Loshchilov and Frank Hutter. Sgdr: Stochastic gradient descent with warm restarts. In *ICLR*, 2017.

- [36] Feifan Lv, Feng Lu, Jianhua Wu, and Chongsoon Lim. Mblen: Low-light image/video enhancement using cnns. In *BMVC*, 2018.
- [37] Long Ma, Tengyu Ma, Risheng Liu, Xin Fan, and Zhongxuan Luo. Toward fast, flexible, and robust low-light image enhancement. In *CVPR*, 2022.
- [38] Sean Moran, Pierre Marza, Steven McDonagh, Sarah Parisot, and Gregory Slabaugh. Deeplpf: Deep local parametric filters for image enhancement. In *CVPR*, 2020.
- [39] Adam Paszke, Sam Gross, Francisco Massa, Adam Lerer, James Bradbury, Gregory Chanan, Trevor Killeen, Zeming Lin, Natalia Gimelshein, Luca Antiga, et al. Pytorch: An imperative style, high-performance deep learning library. In *NeurIPS*, 2019.
- [40] Etta D Pisano, Shuquan Zong, Bradley M Hemminger, Marla DeLuca, R Eugene Johnston, Keith Muller, M Patricia Braeuning, and Stephen M Pizer. Contrast limited adaptive histogram equalization image processing to improve the detection of simulated spiculations in dense mammograms. *Journal of Digital imaging*, 1998.
- [41] Stephen M Pizer, E Philip Amburn, John D Austin, Robert Cromartie, Ari Geselowitz, Trey Greer, Bart ter Haar Romeny, John B Zimmerman, and Karel Zuiderveld. Adaptive histogram equalization and its variations. *Computer vision, graphics, and image processing*, 1987.
- [42] Shanto Rahman, Md Mostafijur Rahman, Mohammad Abdullah-Al-Wadud, Golam Dastagir Al-Quaderi, and Mohammad Shoyaib. An adaptive gamma correction for image enhancement. *EURASIP Journal on Image and Video Processing*, 2016.
- [43] Joseph Redmon and Ali Farhadi. Yolov3: An incremental improvement. *arXiv preprint arXiv:1804.02767*, 2018.
- [44] Olaf Ronneberger, Philipp Fischer, Thomas Brox, a, and b. U-net: Convolutional networks for biomedical image segmentation. In *MICCAI*, 2015.
- [45] Aashish Sharma and Robby T Tan. Nighttime visibility enhancement by increasing the dynamic range and suppression of light effects. In *CVPR*, 2021.
- [46] Ashish Vaswani, Noam Shazeer, Niki Parmar, Jakob Uszkoreit, Llion Jones, Aidan N Gomez, Łukasz Kaiser, and Illia Polosukhin. Attention is all you need. In *NeurIPS*, 2017.
- [47] Ruixing Wang, Xiaogang Xu, Chi-Wing Fu, Jiangbo Lu, Bei Yu, and Jiaya Jia. Seeing dynamic scene in the dark: A high-quality video dataset with mechatronic alignment. In *ICCV*, 2021.
- [48] Ruixing Wang, Qing Zhang, Chi-Wing Fu, Xiaoyong Shen, Wei-Shi Zheng, and Jiaya Jia. Underexposed photo enhancement using deep illumination estimation. In *CVPR*, 2019.
- [49] Shuhang Wang, Jin Zheng, Hai-Miao Hu, and Bo Li. Naturalness preserved enhancement algorithm for non-uniform illumination images. *TIP*, 2013.
- [50] Zhou Wang, Alan C Bovik, Hamid R Sheikh, and Eero P Simoncelli. Image quality assessment: from error visibility to structural similarity. *TIP*, 2004.
- [51] Zhendong Wang, Xiaodong Cun, Jianmin Bao, and Jianzhuang Liu. Uformer: A general u-shaped transformer for image restoration. In *CVPR*, 2022.
- [52] Zhi-Guo Wang, Zhi-Hu Liang, and Chun-Liang Liu. A real-time image processor with combining dynamic contrast ratio enhancement and inverse gamma correction for pdp. *Displays*, 2009.
- [53] Chen Wei, Wenjing Wang, Wenhan Yang, and Jiaying Liu. Deep retinex decomposition for low-light enhancement. In *BMVC*, 2018.
- [54] Bichen Wu, Chenfeng Xu, Xiaoliang Dai, Alvin Wan, Peizhao Zhang, Zhicheng Yan, Masayoshi Tomizuka, Joseph E. Gonzalez, Kurt Keutzer, and Peter Vajda. Visual transformers: Where do transformers really belong in vision models? In *ICCV*, 2021.
- [55] Ke Xu, Xin Yang, Baocai Yin, and Rynson WH Lau. Learning to restore low-light images via decomposition-and-enhancement. In *CVPR*, 2020.
- [56] Xiaogang Xu, Ruixing Wang, Chi-Wing Fu, and Jiaya Jia. Snr-aware low-light image enhancement. In *CVPR*, 2022.
- [57] Wenhan Yang, Shiqi Wang, Yuming Fang, Yue Wang, and Jiaying Liu. Band representation-based semi-supervised low-light image enhancement: Bridging the gap between signal fidelity and perceptual quality. *TIP*, 2021.
- [58] Wenhan Yang, Wenjing Wang, Haofeng Huang, Shiqi Wang, and Jiaying Liu. Sparse gradient regularized deep retinex network for robust low-light image enhancement. *TIP*, 2021.
- [59] Syed Waqas Zamir, Aditya Arora, Salman Khan, Munawar Hayat, Fahad Shahbaz Khan, and Ming-Hsuan Yang. Restormer: Efficient transformer for high-resolution image restoration. In *CVPR*, 2022.
- [60] Syed Waqas Zamir, Aditya Arora, Salman Khan, Munawar Hayat, Fahad Shahbaz Khan, Ming-Hsuan Yang, and Ling Shao. Learning enriched features for real image restoration and enhancement. In *ECCV*, 2020.
- [61] Nicolas ZCarion, Francisco Massa, Gabriel Synnaeve, Nicolas Usunier, Alexander Kirillov, and Sergey Zagoruyko. Rend-to-end object detection with transformers. In *ECCV*, 2020.
- [62] Hui Zeng, Jianrui Cai, Lida Li, Zisheng Cao, and Lei Zhang. Learning image-adaptive 3d lookup tables for high performance photo enhancement in real-time. *TPAMI*, 2020.
- [63] Bowen Zhang, Shuyang Gu, Bo Zhang, Jianmin Bao, Dong Chen, Fang Wen, Yong Wang, and Baining Guo. Styleswin: Transformer-based gan for high-resolution image generation. In *CVPR*, 2022.
- [64] Yonghua Zhang, Xiaojie Guo, Jiayi Ma, Wei Liu, and Jiawan Zhang. Beyond brightening low-light images. *IJCV*, 2021.
- [65] Yonghua Zhang, Jiawan Zhang, and Xiaojie Guo. Kindling the darkness: A practical low-light image enhancer. In *ACM MM*, 2019.
- [66] Sixiao Zheng, Jiachen Lu, Hengshuang Zhao, Xiatian Zhu, Zekun Luo, Yabiao Wang, Yanwei Fu, Jianfeng Feng, Tao Xiang, Philip H.S. Torr, and Li Zhang. Rethinking semantic segmentation from a sequence-to-sequence perspective with transformers. In *CVPR*, 2021.
- [67] Shangchen Zhou, Chongyi Li, and Chen Change Loy. Led-net: Joint low-light enhancement and deblurring in the dark. In *ECCV*, 2022.